WIND ENERGY
Wind Energ. 0000; **00**:1–16
DOI: 10.1002/we

RESEARCH ARTICLE

Conceptual study of a gearbox fault detection method applied on a 5 MW spar type floating wind turbine

Amir R. Nejad [1], Peter Fogh Odgaard[2] and Torgeir Moan[3]

[1]Department of Marine Technology, Norwegian University of Science and Technology (NTNU), NO-7491, Trondheim, Norway
[2]Department of Electronic Systems, Aalborg University, Denmark
[3]Center for Autonomous Marine Operations and Systems (AMOS), Department of Marine Technology, Norwegian University of Science and Technology (NTNU), NO-7491, Trondheim, Norway

ABSTRACT

In this paper a model-based fault detection method for fault detection of gearboxes in offshore wind turbines is presented. The main aim of this paper is to support conceptual studies with more emphasis on early fault detection methods for floating wind turbines. The method is introduced and applied on a 5 MW reference gearbox installed on a spar type floating wind turbine. Faults applied on the main bearing, high and intermediate speed shaft bearings and the planet bearing are examined with this method. The gearbox is modelled in a multi-body simulation environment with high fidelity. The 5 MW gearbox model used in this study is an offshore reference gearbox consists of three stages, two planetary and one parallel stages, which is supported in a 4- points configuration layout. The bearing faults are detected through the angular velocity error function. The angular velocity measurements are carried out at input, output shafts and two additional sensors inside the gearbox. The aim of the method is also to detect the fault through the external sensors - input and output shafts - measurements, which can be embedded in the existing control system. The results reveal the possibility of early fault detection by this method for large floating wind turbines.

KEYWORDS

Wind turbine gearbox, Condition monitoring, Fault detection, Spar Floating Wind Turbine

Correspondence

Department of Marine Technology, Norwegian University of Science and Technology, NO-7491, Trondheim, Norway. E-mail: Amir.Nejad@ntnu.no

Received . . .

1. INTRODUCTION

Drivetrains in wind turbines are used to convert the wind's kinetic energy to the electrical power. Experiences [1] show that faults or damages in the drivetrain contribute significantly to the wind turbine's downtime and non-availability. The maintenance and repair is particularly too costly for the offshore wind turbines where special vessel and crane barge is needed to replace the faulty drivetrain. In addition, the harsh offshore weather reduces the repair period only to few

Prepared using weauth.cls [Version: 2010/06/17 v1.00]

months often in summers. There is therefore a need to develop reliable tools and methods for condition monitoring and fault detection of the wind turbine's components.

The condition monitoring is based on the fact that an emerging defect is detected from the changes in the system's conditions. For gears for instance, crack damage can be detected from the torsional vibration due to changes in tooth mesh stiffness [2, 3, 4]. The condition monitoring and fault diagnosis system can be embedded in control system, for instance for blade pitch actuators [5], or can be a separate system. The most common methods for the drivetrain condition monitoring include vibration [4, 6, 7], temperature, noise and oil particle measurements [8, 9] which are often not integrated in the classical wind turbine control system. Lu et al. [10], Hameed et al. [11] and Yang et al. [12] have provided a comprehensive review of methods used for the gearbox condition monitoring in wind turbines. Isermann [13] has classified the condition monitoring in three groups of monitoring, automatic protection and supervision. The monitoring and automatic protection are the limit-value based methods where the alarm or corrective actions are implemented as soon as a threshold is passed. Quick response, reliability and simplicity are indeed the most advantages of these methods, while the disadvantage is that they act only when a considerable change has already occurred in the system [13]. The fault diagnostic methods at supervision level are expected to detect the fault in an early stage of development. This in general can be achieved by evaluating the trend in measurements. Any information about the system or having a model of the system is a great advantage as it can provide a deep insight into the system behaviour [13, 14, 15].

For drivetrains in wind turbines, methods that can detect faults in an early stage are very advantageous and cost-effective especially if the monitoring system can also employ existing sensors. Oil debris analysis [16] or thermography [17] analysis are often used as offline systems in periodic inspections [18, 19]. The simple torsional model proposed by Perišić et al. [20] is of interest for detecting the faults in the rotor in a model-based monitoring system. However, this method is unlikely to capture faults inside the drivetrain or bearings as they are not included in the model.

The common approach for the drivetrain fault detection is to employ a vibration-based condition monitoring system. In this method the accelerometers are installed on three locations on the wind turbine drivetrain housing [21], near the main shaft, in the middle and near the generator shaft - see Figure 1.

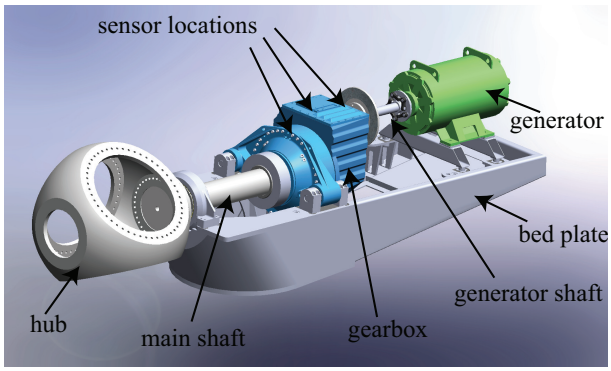

Figure 1. Measuring locations on gearbox as recommended by ISO 10816-21 [21] - figure adapted from Nejad et al. [22].

The main goal of such systems are to ensure that the system operates within the acceptable vibration limits. As the vibration amplitudes (often measured in terms of rms of velocity or acceleration) pass the limits suggested by standards such as ISO 10816-21 [21] or manufacturers guideline, an alarm is generated. There are in general two issues with this approach. First, the vibration-based fault detection is not a system integrated within the control system at the time of manufacturing. It is an optional system with additional cost and often is not supplied by the drivetrain manufacturer, but by a separate company with another contract and financial terms. Many existing wind turbines are not fitted with such systems. Second, more sensors are needed to identify exactly the root cause of the failure as there are many gears and bearings inside the gearbox with wide range of frequency. Faults in gears and bearings are normally seen in their mesh frequencies and their harmonics.

Wind Energ. 0000; **00**:1–16 © 0000 John Wiley & Sons, Ltd.
DOI: 10.1002/we
Prepared using weauth.cls

Nejad et al. [23] and Odgaard and Nejad [24] proposed a simple vibration-based fault detection approach employing the existing sensors within the existing control system. The goal was to minimize the additional cost for a separate condition monitoring system. The proposed method employs angular velocity measurements from the input and output shafts, which are often standard measurements in existing control system, and two additional angular velocity measurements from the intermediate shaft inside the gearbox. The concept is based on the dynamic transmission error known in gear systems [23]. The method was tested on a high fidelity wind turbine drivetrain model (750 kW) and found to be accurate enough to identify some of the bearing defects prior to failure and system damage [23]. The 750 kW drivetrain used in this initial study was installed on a land-based wind turbine.

In previous studies [25, 26], it was shown that the drivetrain on floating wind turbines are subjected to different loading/motion conditions than those on land-based ones. The wave induced motion in floating wind turbines causes dynamic forces which are transferred through drivetrain. Moreover, large multi-megawatt wind turbine drivetrains follow fundamentally different design approach than the small size drivetrains [27]. Therefore, this study is aimed to evaluate the possibility of employing of the angular velocity error function method as introduced by authors [23] on the drivetrains on large floating wind turbines. Based on the results of a previous study [25] of several 5 MW floating wind turbine designs (a TLP, two semi-submersibles and a spar), the spar was chosen for further examination due to its relatively large motion, axial force, and nacelle acceleration. Thus, the 5 MW reference gearbox [27] used in this study is installed on a spar type floating wind turbine. The gearbox is modelled in a multi body simulation (MBS) tools and simulations are conducted for the rated wind speed where the turbine produced its rated power. The de-coupled approach is employed in this study meaning that the forces and moments obtained from global analysis are applied on the main shaft in MBS model. Bearing faults are introduced in each stage of the gearbox and the error function method is applied for detection.

2. WIND TURBINE & DRIVETRAIN MODELS

A 5 MW reference gearbox [27] mounted on the floating OC3 Hywind spar structure [28, 29] is used in this study. This wind turbine is a 3-bladed upwind turbine with rated wind speed of 12.1 rpm. The spar floating structure is a column shaped structure which is connected by mooring lines to the seabed. The details of the spar structure used in this paper can be found in Nejad et al. [25].

The 5-MW reference gearbox used in this study was developed by Nejad et al. [27] for offshore wind turbines. This gearbox follows the most conventional design types of those used in wind turbines. The gearbox consists of three stages, two planetary and one parallel stage gears. Table I shows the general specifications of this gearbox. The gearbox was designed with a 4-point support with two main bearings to reduce non-torque loads entering the gearbox.

The MBS model of this gearbox is presented in Figure 2 using the commercial software, SIMPACK [30]. In this model, bearings are modelled by their stiffness. Gears are modelled by SIMPACK gear pair element which considers, among others, involute meshing teeth and parabolic behavior of tooth stiffness. More details about the gear pair model in SIMPACK can be found for example in Ebrahimi and Eberhard [31].

As it is shown in the figure, the motions are applied on the bed plate and the external loads on the main shaft. The generator torque and speed is then controlled at the generator side [27].

3. METHODOLOGY

3.1. De-coupled Approach & Environmental Condition

The dynamic excitations of wind turbine gearboxes are classified into external and internal groups. The external excitations—including wind and wave—are in low frequency range, often less than 2 Hz. The external excitations include also the dynamic loads on main shaft induced by the vibration of the whole wind turbine system such as tower bending

Table I. 5-MW reference gearbox specification [27].

Parameter	Value
Type	2 Planetary + 1 Parallel
1st stage ratio	1:3.947
2nd stage ratio	1:6.167
3rd stage ratio	1:3.958
Total ratio	1:96.354
Designed power (kW)	5000
Rated input shaft speed (rpm)	12.1
Rated generator shaft speed (rpm)	1165.9
Rated input shaft torque (kN.m)	3946
Rated generator shaft torque (kN.m)	40.953
Total dry mass ($\times$1000 kg)	53
Service life (year)	20

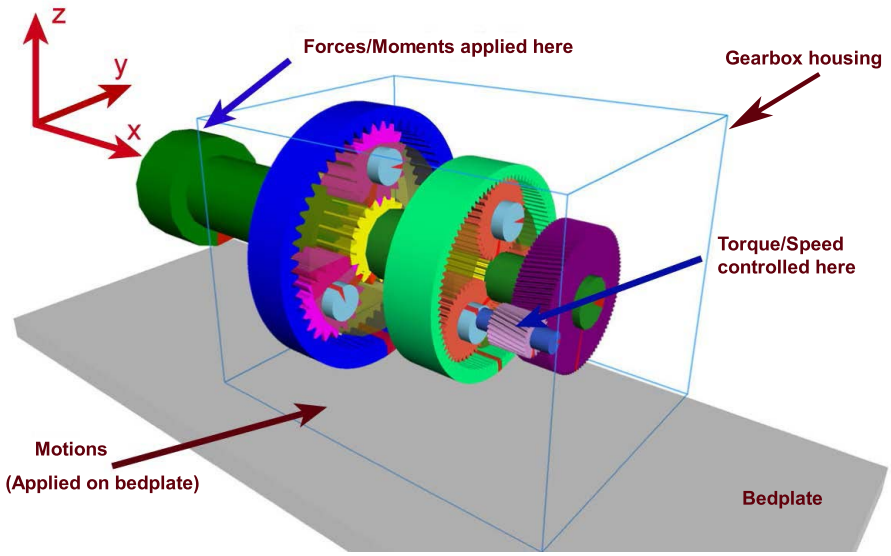

Figure 2. MBS model of the 5-MW reference gearbox [27].

or blade bending. The gear mesh frequencies, which cause internal excitations, are normally in the high frequency range, above 20 Hz. Therefore, in order to capture the internal resonances, simulations with very small time steps (e.g. 0.005 s) are required, while simulations with 0.1 s can often capture possible responses to external excitations.

The external excitations occur at integer multiples of rotor speed. The internal excitation occurs at gear mesh frequencies, f_m, which for simple parallel spur or helical gears are defined as [32]:

$$f_m = \frac{N_{gear} Z}{60} \tag{1}$$

in which N_{gear} is the gear rotational speed in rpm and Z is the number of teeth. For planetary gears more complicated formula is used for the mesh frequency calculation - see for instance AGMA 6123-C16 [33] or McFadden [34]. Harmonics, at integer multiplies of mesh frequencies, and sidebands often occurs [32, 35].

Wind Energ. 0000; **00**:1–16 © 0000 John Wiley & Sons, Ltd.
DOI: 10.1002/we
Prepared using weauth.cls

The different simulation frequency requirements as well as the computational requirements for complex gearbox models encourage using a "de-coupled" analysis approach. Figure 3 presents a schematic procedure of the de-coupled analysis approach for wind turbine gearbox analysis.

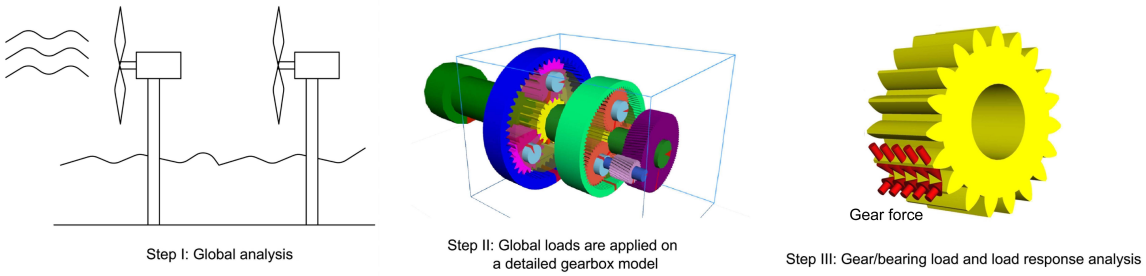

Figure 3. Drivetrain de-coupled analysis method.

First, the forces and moments on the main shaft are obtained from the global response analysis. Second, they are used as inputs to a detailed gearbox model in a Multi Body Simulation (MBS) model where simulations with a higher fidelity model and smaller time steps are carried out.

The global analysis is conducted by using an aero-hydro-servo-elastic code, SIMO-RIFLEX-AeroDyn [36]. simulations are carried out at the rated wind speed with wave conditions characterized by significant wave height $H_S = 5$ m and peak period $T_P = 12$ s (modelled by a JONSWAP spectrum). The turbulence intensity factor is taken as 0.15 according to IEC 61400-1 [37]. The environmental data used in this study were generated by a numerical hindcast model at the National and Kapodistrian University of Athens (NKUA), which corresponds to the data from a buoy off the coast of Portugal [38]. The data was hourly sampled and generated from a hindcast model from 2001 to 2010. Long-term joint distributions of the mean wind speed (U_w), significant wave height (H_s) and spectral peak period (T_p) were obtained by fitting analytical distributions with the hindcast data. The joint distribution of U_w, H_s, and T_p (Eq. 2) consists of a marginal distribution of U_w (with two-parameter Weibull distribution), a conditional distribution of H_s given U_w (with two-parameter Weibull distribution), and a conditional distribution of T_p given both U_w and H_s which follows a lognormal distribution [38].

$$f_{U_w,H_s,T_p}(u,h,t) = f_{U_w}(u) \cdot f_{H_s|U_w}(h|u) \cdot f_{T_p|U_w,H_s}(t|u,h) \tag{2}$$

where $f()$ refers to probability density function (PDF). The fitting methods and the parameters for the joint distribution at this site can be found in Li et al. [38].

To minimize the statistical uncertainties, six 3800 s simulations are carried out for each wind speed. The first 200 s are removed during post-processing to avoid start-up transient effects. The sampling frequency is 200 Hz, thus the simulation does not include the gear mesh component at the high speed shaft.

In the MBS analysis, bearings are modelled as force elements and their force-deflection relation. Gears are modelled with compliance at tooth including detailed tooth properties [27]. The generator should also be modelled. The generator model depends on the choice of the generator. Synchronous generators act as power-dependent torsional springs, whereas asynchronous or induction generators are modelled by dampers in operating conditions or free-free lumped masses [39]. In this paper a doubly fed induction generator (DFIG) is considered and modelled. Doubly fed induction generators are the ones mostly used in wind turbines [40].

The de-coupled method described above has been used in this paper. Earlier works on wind turbine gearboxes based on the de-coupled method include, for instance Xing et al. [41], Dong et al. [42], Jiang et al. [43] and Nejad et al. [44].

3.2. Fault Cases

A set of bearings from the case study gearbox are chosen for the fault study. They are selected based on their probability of fatigue failure and vulnerability map as described by Nejad et al. [27, 26]. The bearing damage is modelled by varying the bearing's deflection in the axial or radial directions. This is done by changing the bearing stiffness in different directions. As the bearing degrades the stiffness reduces and therefore the relative displacement increases. This approach of bearing fault modelling is discussed in Nejad et al. [23] and Ghane et al. [45].

Figure 4 and Table II present the fault cases studied in this paper. For INP-B, the axial deflection is changed from 2.5×10^{-3} mm to 2.5×10^{-2} mm for each 1 kN applied force. In LC2, HS-A, and LC3, IMS-B, the deflection is changed from 1.2×10^{-3} mm to 1.2×10^{-1} mm, and for LC4, the radial deformation is reduced from 8.3×10^{-4} mm to 8.3×10^{-2} mm for each 1 kN applied force.

Table II. Fault cases

Fault case	Description
LC0	Reference case, fault-free
LC1	Damage in axial direction of the down wind main bearing (INP-B)
LC2	Damage in radial direction of the high-speed shaft bearing (HS-A)
LC3	Damage in radial direction of the intermediate-speed shaft bearing (IMS-B)
LC4	Damage in radial direction of the 2nd stage planet bearing (IMS-PL-A)

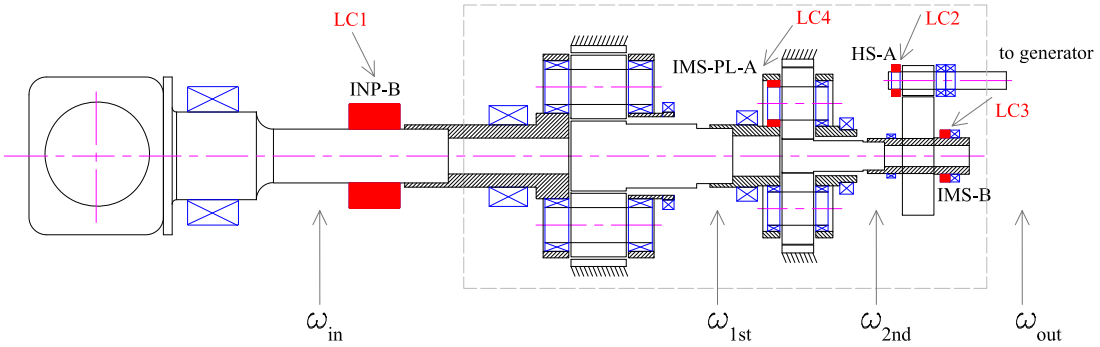

Figure 4. Fault cases and the angular velocity measurement locations.

The angular velocity error functions [23] as defined in following equations (equations 3 - 6) are used for fault detections.

$$e_t = \omega_{out} - \alpha\omega_{in} \tag{3}$$

$$e_{12} = \omega_{1st} - \alpha_1\omega_{in} \tag{4}$$

$$e_{23} = \omega_{2nd} - \alpha_2\omega_{1st} \tag{5}$$

$$e_{3o} = \omega_{out} - \alpha_3\omega_{2nd} \tag{6}$$

In these equations, α, α_1, α_2 and α_3 are the inverse of the gear ratios (see Table I) and ω represent angular velocities shown in Figure 4. As it is seen in the equations, e_t uses the measurements of angular velocities at input and output of the gearbox, while other error functions require additional measuring sensors inside the gearbox.

Wind Energ. 0000; **00**:1–16 © 0000 John Wiley & Sons, Ltd.
DOI: 10.1002/we
Prepared using weauth.cls

The faults in the gearbox change the error function which can be detected by the reference values known for instance from the MBS model simulation or real measurements. Moreover, studying the long-term error function and comparison with the model can reveal the behaviour of the system and prevent potential failures. Table III summarizes the required measurements and error function comparison for each fault case.

Table III. Measurements & error functions

Fault case	Measurements	Error functions	Detection
LC0	$\omega_{in}, \omega_{out}, \omega_{1st}, \omega_{2nd}$	$e_t, e_{12}, e_{23}, e_{3o}$	reference values
LC1	$\omega_{in}, \omega_{out}, \omega_{1st}$	e_t, e_{12}	compare e_t, e_{12} with reference values
LC2	$\omega_{in}, \omega_{out}, \omega_{2nd}$	e_t, e_{3o}	compare e_t, e_{3o} with reference values
LC3	$\omega_{in}, \omega_{out}, \omega_{2nd}$	e_t, e_{3o}	compare e_t, e_{3o} with reference values
LC4	$\omega_{in}, \omega_{out}, \omega_{1st}, \omega_{2nd}$	e_t, e_{23}	compare e_t, e_{23} with reference values

3.3. Frequency based detection scheme

In this paper, an updated version of the frequency based detection scheme presented by Odgaard and Stoustrup [46, 47] is employed. This approach is primarily based on the detection of the changed resonance frequencies due to faults which are compared with the normal fault free case.

In order to select a suited base for distinguishing certain phenomena in time, frequency or time/frequency domains, it is important to find a base which supports the phenomenon in question. In this case the problem is to detect a changing resonance frequency, a windowed fast Fourier transform (FFT) or Cosine base would be relevant as it supports the frequency content for at given window length, and the frequency content would change with time as the fault develops. The window length should be selected such that short time variations in the operation is levelled out, while short enough to detect changes in frequency content of the measurements, like changes in different resonance frequencies. The frequency responses obtained by the windowed FFT algorithm would subsequently be compared to determine if the response is as expected. The problem with such a scheme is that it is relatively computationally demanding. One solution to reduce the computational time is to design band pass filters which has pass band in the frequency range which is changed in case of a given fault [46, 47]. This filter is used to compute energy in the measurements in this frequency range. This energy content is subsequently normalized with the energy in the signal for the given window length. It is assumed that a certain energy level will be present at a given frequency of f (e.g. due to resonance frequency) and the signal on which the frequency detection should be applied, $y[n]$, can be defined.

The first step in this approach is to extract the energy in the signal at the requested frequency by a band pass filter, $H_f[z]$. This filter is subsequently applied to the signal $y[n]$ to obtain $y_{Hf}[n]$.

The next step is to compute the energy in the signals for a given window length, L. The energies, $E_{Hf}[n]$, for the energy in the band pass filtered signal, and $E[n]$ the energy in the normal signal, are computed as:

$$E_{Hf}[n] = \mathbf{y}_{Hf}[n] \cdot \mathbf{y}_{Hf}[n]^T, \tag{7}$$

$$E[n] = \mathbf{y}[n] \cdot \mathbf{y}[n]^T, \tag{8}$$

in which,

$$\mathbf{y}_{Hf}[n] = \begin{bmatrix} y_{Hf}[n-(L-1)] & \cdots & y_{Hf}[n] \end{bmatrix}, \tag{9}$$

$$\mathbf{y}[n] = \begin{bmatrix} y[n-(L-1)] & \cdots & y[n] \end{bmatrix}. \tag{10}$$

DOI: 10.1002/we
Prepared using weauth.cls

Subsequently a ratio, $\gamma[n]$, between these two energies can be computed to detect changes in energy level.

$$\gamma[n] = \frac{E_{Hf}[n]}{E[n]}. \tag{11}$$

This ratio $\gamma[n]$ - which is called hereafter in this paper as the detection value - will subsequently be compared with a threshold κ. The value of the κ should be found based on real data, and is selected such that the fault is detected early, but still without a high number of false positive detections.

4. RESULTS & DISCUSSIONS

The proposed detection scheme is applied on the case study and results are presented in this section. For each fault, two questions should be answered: is it possible to detect this fault by using the proposed scheme? Secondly, is there a difference between using the error function from external speed measurements (e_t) and the error function from internal speed measurements (e_{12}, e_{23} and e_{3o})? The latter set of measurements requires additional sensors inside the gearbox, while the external speed measurements are often available in the existing control system. Therefore, the use of external speed measurements is preferred.

The FFT of the angular velocity error functions for LC1 to LC4 with the reference values from LC0 are plotted in Figures 5 - 12. Since these faults are related to bearings wear, it is reasonable to assume that they develop slowly and the transient phase between fault and non-fault scenario can be ignored. Therefore, datasets with faults or datasets with non-faults are only used in this study.

It should be noted that the frequencies shown in following figures are related to the gear mesh frequencies. The angular velocity error function is dominated by tooth-tooth meshing frequencies. This is inline with the results of earlier studies, for instance for bearing faults [48] or gear faults [4].

4.1. Analysis of variable resonance frequencies

The FFT of the angular velocity error functions for fault and non-fault cases are analysed and commented in this section.

LC1 For this load case, the FFT of the angular velocity error function e_{12} is plotted in Figure 5 and the error function obtained from external speed measurements, e_t is shown in Figure 6. Form both figures, it is evident that it is not possible to detect the fault in LC1 from any of these two data. No filter is designed for this case as it is not possible to distinguish LC1 from LC0 in the frequency domain.

LC2 The FFT of angular velocity error functions from internal and external speed measurements (e_{3o} and e_t) for load case LC2 are compared with LC0 in Figs. 7 - 8. These figures show that the LC2 fault can be detected in the frequency range of 44.5 Hz - 45 Hz. A bandpass filter is subsequently designed for this frequency range for fault detection related to LC2 case.

LC3 The LC3 FFTs of the angular velocity error functions e_{3o} and e_t are compared with the LC0 in Figs. 9 - 10. From the figures it can be seen that the fault detection might be possible with both error function data in the frequency range between 42.4 Hz and 43.4 Hz. Therefore, a bandpass filter is designed for this frequency range related to LC3 fault.

LC4 The angular velocity error functions FFTs of the e_{23} and e_t compared with the LC0 are presented in Figs. 11 - 12. Figures indicate possibility of detection in the frequency range between 30 Hz and 70 Hz. A bandpass filter is designed for a more narrow frequency range between 49.5 Hz and 52 Hz for this fault case.

Wind Energ. 0000; **00**:1–16 © 0000 John Wiley & Sons, Ltd.
DOI: 10.1002/we
Prepared using weauth.cls

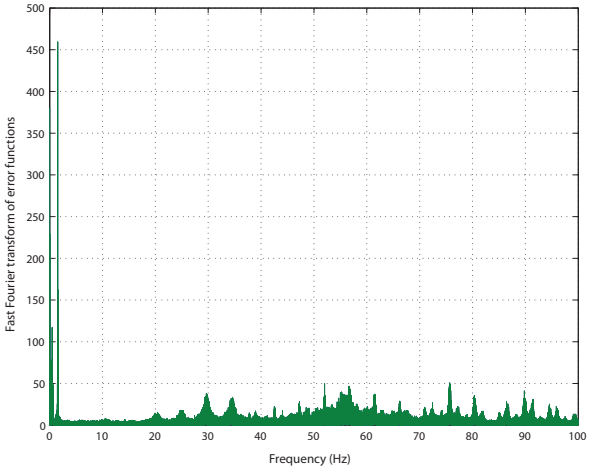

Figure 5. Frequency content of e_{12} for LC1 (green) and LC0 (blue).

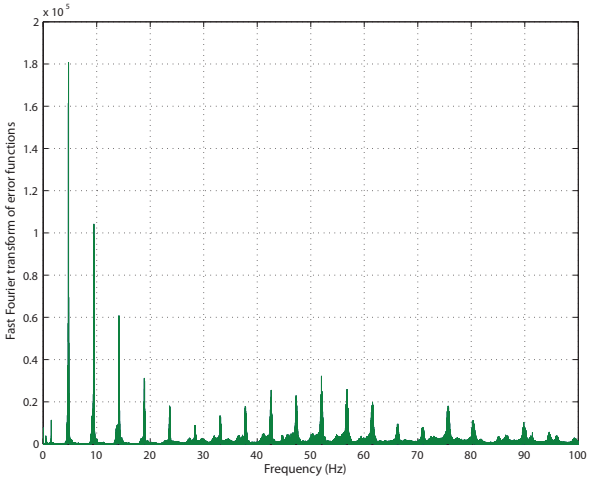

Figure 6. Frequency content of e_t for LC1 (green) and LC0 (blue).

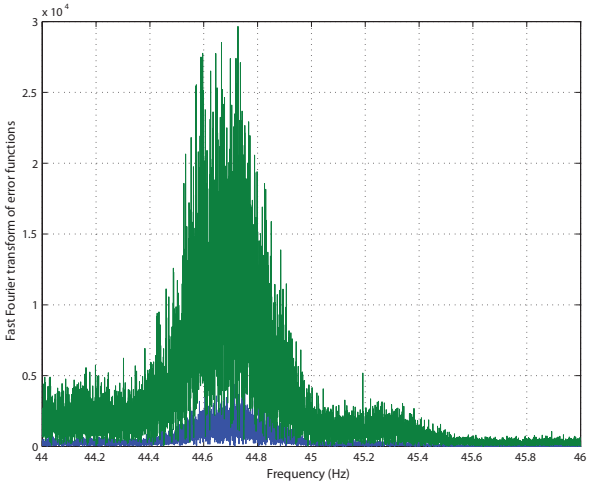

Figure 7. Frequency content of e_{3o} for LC2 (green) and LC0 (blue).

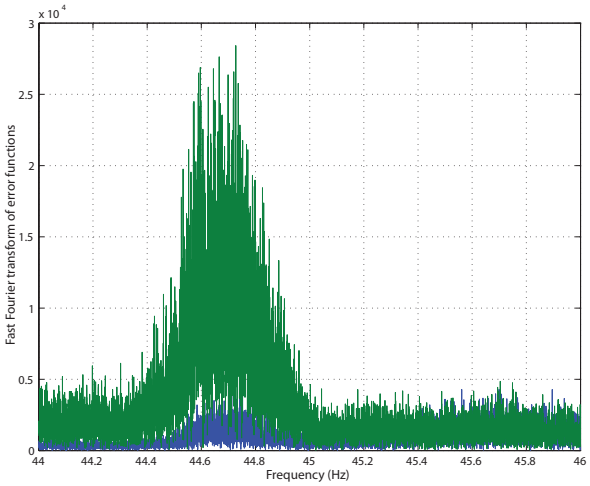

Figure 8. Frequency content of e_t for LC2 (green) and LC0 (blue).

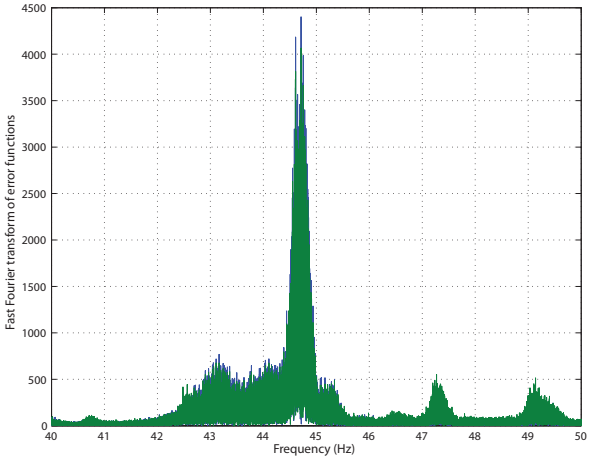

Figure 9. Frequency content of e_{3o} for LC3 (green) and LC0 (blue).

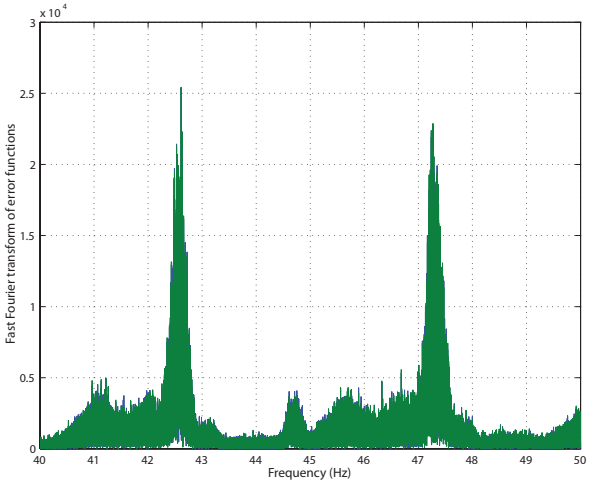

Figure 10. Frequency content of e_t for LC3 (green) and LC0 (blue).

Wind Energ. 0000; **00**:1–16 © 0000 John Wiley & Sons, Ltd.
DOI: 10.1002/we
Prepared using weauth.cls

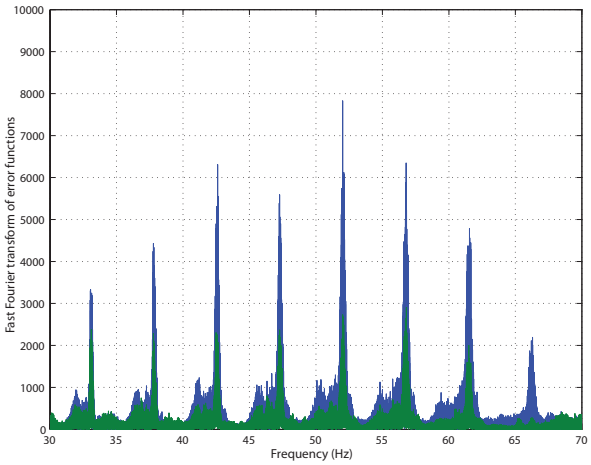

Figure 11. Frequency content of e_{23} for LC4 (green) and LC0 (blue).

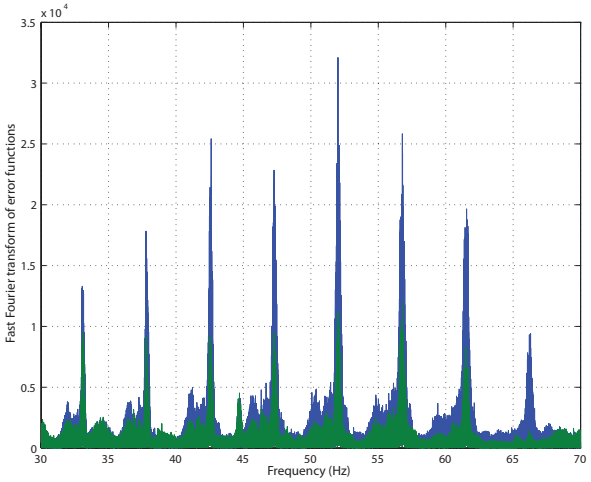

Figure 12. Frequency content of e_t for LC4 (green) and LC0 (blue).

4.2. Detection results

Using the detection scheme described in section 3.3, the possibility of detection using different detection filters on different error functions is discussed. The detection values as calculated by equation 11 are presented in Table IV for all angular velocity error functions in the non-fault case LC0. These are the reference values which are used as references for the fault cases LC1 - LC4. The detection values presented for LC1 to LC4 in Tables V to VIII are shown in normalized values with respect to reference values given in Table IV.

Table IV. Detection values for LC0 (reference values).

Error function	Filter LC2	Filter LC3	Filter LC4
e_t	$1.2700 \cdot 10^{-2}$	$2.6240 \cdot 10^{-1}$	$5.6610 \cdot 10^{-1}$
e_{12}	$1.0803 \cdot 10^{-7}$	$3.1239 \cdot 10^{-7}$	$2.7467 \cdot 10^{-6}$
e_{3o}	$1.2600 \cdot 10^{-2}$	$7.0826 \cdot 10^{-4}$	$8.9743 \cdot 10^{-5}$
e_{23}	$5.2713 \cdot 10^{-5}$	$1.6200 \cdot 10^{-2}$	$3.4000 \cdot 10^{-2}$

In Table V, the detection values for the three filters and the error functions are presented for LC1 case. Similar to the results from frequency domain, it is evident that the detection is not possible for this fault case. It can be seen from the

table that the values of the detection signals are similar to the ones from the reference values thus there is no false positive detection for LC1 case.

Table V. Normalised detection values for LC1.

Error function	Filter LC2	Filter LC3	Filter LC4
e_t	1.00	1.00	1.00
e_{12}	1.00	1.00	1.00

The normalised detection values for error functions related to LC2 are presented in Table VI. The detection values for both e_t, which uses external measurements, and e_{3o} , using internal measurements, are considerably higher than reference values which indicates that detection is possible for this fault case. It should be noted that the false positive detections of the other faults is avoided as the LC2 filter is only active in this fault case.

Table VI. Normalised detection values for LC2.

Error function	Filter LC2	Filter LC3	Filter LC4
e_t	**51.34**	1.13	1.04
e_{3o}	**55.59**	57.75	9.27

Comparison results for LC3 fault case is presented in Table VII. The changes in detection values with respect to reference values are too small to be able to detect this fault case.

Table VII. Normalised detection values for LC3.

Error function	Filter LC2	Filter LC3	Filter LC4
e_t	0.83	**0.99**	0.99
e_{3o}	0.83	**0.87**	1.88

The results of the detection values for LC4 is presented in Table VIII for the three filters and the error functions. The changes in detection values are considerable and thus the fault detection is possible by using either of e_t or e_{23}.

Table VIII. Normalised detection values for LC4.

Error function	Filter LC2	Filter LC3	Filter LC4
e_t	0.89	0.17	**0.18**
e_{23}	0.86	0.17	**0.18**

4.3. Discussions

From the results, it is evident that the fault cases LC2 and LC4 were detected by the proposed method, while this method was not suitable for detection of the cases in LC1 and LC3. Referring to Table II, LC2 and LC4 are related to the damage in the high-speed shaft bearing and the second stage planet bearing respectively. The reason that LC2 and LC4 were detectable by this method lies on the physics of this detection method. The fault in bearings in LC2 and LC4 are in radial direction meaning that their faults create an excitation in radial direction, similar to an unbalanced mass system. This radial excitation can be seen in the rotational angular velocity and therefore the proposed method, which is based on the angular velocity measurement, is able to detect them.

The fault in LC3 is also in radial direction, but why the proposed method was not able to detect this fault case? The LC3 is the fault case in bearing IMS-B located at the end of the intermediate-speed shaft. There is also one more bearing (IMS-A) near to this faulty bearing - see Figure 4. These are taper type bearings and normally are installed together. The reason that the fault in LC3 was not detected is because of this nearby bearing which has carried the additional loads caused by fault in IMS-B, and thus no or very little vibration is produced.

DOI: 10.1002/we
Prepared using weauth.cls

The LC1 case was not detectable by the proposed method because the fault in this case is in the axial direction and therefore affects the axial vibration which is not seen in the rotational velocity signals. Other methods - for example evaluating the axial acceleration - is needed to detect such axial faults [49].

It is also interesting to note that the faults in LC2 and LC4 can be detected by using either external measurements or internal measurements. As discussed earlier the external measurements are preferred as these are often existing sensors already installed with the control system.

5. CONCLUDING REMARKS

In this paper, a model-based method was demonstrated and applied on a 5 MW reference gearbox installed on a spar type floating wind turbine. The proposed detection method is based on the angular velocity error function and measurements of the angular velocity of input and output shafts. A detailed multi body model of the gearbox was used and simulations were conducted at rated wind speed and associated wave data taken from the most probable environmental condition measured at a site off the coast of Portugal. A de-coupled approach was employed to calculate the global load effects which were then used and applied on the gearbox model for local analysis and fault detection examination. Bearings faults were introduced by altering the bearing force-deflection properties, representing the wear and damage inside the bearing.

The main aim was firstly to investigate the potential of using gearbox speed measurements for gearbox fault diagnosis in floating wind turbines as a replacement for expensive add-on condition monitoring systems. Secondly, a frequency model based filter approach was applied on the case study wind turbine. The fault cases in LC2 and LC4 were detected by the proposed method, while this method was not suitable for detection of the cases in LC1 and LC3. LC2, LC3 and LC4 are related to the faults in radial direction of bearings and LC1 covers a fault in the axial direction. It was observed that the proposed method is suitable for detecting bearings' damage in the radial direction, but not effective for the faults in the axial direction. The LC3, which was a case with fault in the radial direction, was not detected due to existence of a nearby bearing covering the additional loads caused by this fault case.

It is also important to see the modulation of the gear mesh frequencies and bearing faults. In other words, this article demonstrates the influence of bearing damage on the modulation of the gear tooth harmonics by using the changes to the angular velocity fluctuations.

A similar approach, using the shaft angular velocity for the gearbox fault detection, was tested by Roy et al. [50] on a small size gearbox with a known fault. Employing the error function method, as described in present article, has so far been extensively tested on high fidelity models (750 kW and 5 MW) on both land-based and floating wind turbines with different drivetrain configurations and different fault levels. In the next step and with collaboration with an industrial partner, a test wind turbine drivetrain is planned to be used for experimental evaluation of the proposed method.

ACKNOWLEDGEMENTS

This work was partly supported by the Research Council of Norway through the Centres of Excellence funding scheme, Project number 223254 - AMOS - at Department of Marine Technology, Norwegian University of Science and Technology (NTNU).

REFERENCES

1. S. Faulstich, B. Hahn, and P.J. Tavner. Wind turbine downtime and its importance for offshore deployment. *Wind Energy*, 14:327–337, 2011.

2. Shengxiang Jia and Ian Howard. Comparison of localised spalling and crack damage from dynamic modelling of spur gear vibrations. *Mechanical Systems and Signal Processing*, 20(2):332–349, 2006.
3. Song Xue, Rodney Entwistle, Ilyas Mazhar, and Ian Howard. The spur planetary gear torsional stiffness and its crack sensitivity under quasi-static conditions. *Engineering Failure Analysis*, 63:106 – 120, 2016.
4. Song Xue and Ian Howard. Torsional vibration signal analysis as a diagnostic tool for planetary gear fault detection. *Mechanical Systems and Signal Processing*, 100:706–728, 2018.
5. Y. Vidal, C. Tutivén, J. Rodellar, and L. Acho. Fault diagnosis and fault-tolerant control of wind turbines via a discrete time controller with a disturbance compensator. *Energies*, 8(5):4300–4316, 2015.
6. Z. Feng, S. Qin, and M. Liang. Timefrequency analysis based on vold-kalman filter and higher order energy separation for fault diagnosis of wind turbine planetary gearbox under nonstationary conditions. *Renewable Energy*, 85:45 – 56, 2016.
7. J. Igba, K. Alemzadeh, C. Durugbo, and E. T. Eiriksson. Analysing RMS and peak values of vibration signals for condition monitoring of wind turbine gearboxes. *Renewable Energy*, 91:90 – 106, 2016.
8. J. Igba, K. Alemzadeh, C. Durugbo, and K. Henningsen. Performance assessment of wind turbine gearboxes using in-service data: Current approaches and future trends. *Renewable and Sustainable Energy Reviews*, 50:144 – 159, 2015.
9. J. Zhu, J. M. Yoon, D. He, and E. Bechhoefer. Online particle-contaminated lubrication oil condition monitoring and remaining useful life prediction for wind turbines. *Wind Energy*, 18(6):1131–1149, 2015.
10. B. Lu, Y. Li, X. Wu, and Z. Yang. A review of recent advances in wind turbine condition monitoring and fault diagnosis. In *Power Electronics and Machines in Wind Applications, 2009. PEMWA 2009. IEEE*, pages 1–7. IEEE, 2009.
11. Z. Hameed, Y.S. Hong, Y.M. Cho, S.H. Ahn, and C.K. Song. Condition monitoring and fault detection of wind turbines and related algorithms: A review. *Renewable and Sustainable Energy Reviews*, 13(1):1 – 39, 2009.
12. W. Yang, P. J. Tavner, C. J. Crabtree, and M. Wilkinson. Cost-effective condition monitoring for wind turbines. *IEEE Transactions on Industrial Electronics*, 57(1):263–271, 2010.
13. R. Isermann. Model-based fault-detection and diagnosis status and applications. *Annual Reviews in Control*, 29(1):71 – 85, 2005.
14. R. Isermann and P. Ballé. Trends in the application of model-based fault detection and diagnosis of technical processes. *Control Engineering Practice*, 5(5):709 – 719, 1997.
15. Inseok Hwang, Sungwan Kim, Youdan Kim, and Chze Eng Seah. A survey of fault detection, isolation, and reconfiguration methods. *IEEE Transactions on Control Systems Technology*, 18(3):636–653, 2010.
16. Shuangwen Sheng. Monitoring of wind turbine gearbox condition through oil and wear debris analysis: A full-scale testing perspective. *Tribology Transactions*, 59(1):149–162, 2016.
17. MA Drewry and GA Georgiou. A review of NDT techniques for wind turbines. *Insight-Non-Destructive Testing and Condition Monitoring*, 49(3):137–141, 2007.
18. A.R. Nejad, Z. Gao, and T. Moan. Fatigue reliability-based inspection and maintenance planning of gearbox components in wind turbine drivetrains. *Energy Procedia*, 53:248 – 257, 2014.
19. C.J. Hockley. Wind turbine maintenance and topical research questions. *Procedia CIRP*, 11:284 – 286, 2013.
20. Nevena Perišić, Poul Henning Kirkegaard, and Bo Juul Pedersen. Cost-effective shaft torque observer for condition monitoring of wind turbines. *Wind Energy*, 18(1):1–19, 2015.
21. ISO10816-21. Mechanical vibration, evaluation of machine vibration by measurements on non–rotating parts: Horizontal axis wind turbines with gearbox, 2015.
22. A.R. Nejad, Y. Xing, Y. Guo, J. Keller, Z. Gao, and T. Moan. Effect of floating sun gear in wind turbine planetary gearbox with geometrical imperfections. *Wind Energy*, 18(12):2105 2120, 2015.
23. A.R. Nejad, P.F. Odgaard, Z. Gao, and T. Moan. A prognostic method for fault detection in wind turbine drivetrains. *Engineering Failure Analysis*, 42:324 – 336, 2014.

DOI: 10.1002/we
Prepared using weauth.cls

24. P.F. Odgaard and A.R. Nejad. Frequency based wind turbine gearbox fault detection applied to a 750 kw wind turbine. In *Control Applications (CCA), 2014 IEEE Conference on*, pages 1383–1388. IEEE, 2014.
25. A.R. Nejad, E.E. Bachynski, M.I. Kvittem, C. Luan, Z. Gao, and T. Moan. Stochastic Dynamic Load Effect and Fatigue Damage Analysis of Drivetrains in Land-based and TLP, Spar and Semi-Submersible Floating Wind Turbines. *Marine Structures*, 42:137–153, 2015.
26. A.R. Nejad, E.E. Bachynski, Z. Gao, and T. Moan. Fatigue damage comparison of mechanical components in a land-based and a spar floating wind turbine. *Procedia Engineering*, 101:330–338, 2015.
27. A.R. Nejad, Y. Guo, Z. Gao, and T. Moan. Development of a 5 MW reference gearbox for offshore wind turbines. *Wind Energy*, 19(6):1089 – 1106, 2016.
28. J. Jonkman, S. Butterfield, W. Musial, and G. Scott. Definition of a 5-MW reference wind turbine for offshore system development. Technical Report NREL/TP-500-38060, US National Renewable Energy Laboratory (NREL), 2009.
29. J. Jonkman. *Definition of the Floating System for Phase IV of OC3*. National Renewable Energy Laboratory, 2010.
30. SIMPACK. Multi-body simulation software. http://www.simpack.com/. [Online; accessed 10-Mar-2018].
31. Saeed Ebrahimi and Peter Eberhard. Rigid-elastic modeling of meshing gear wheels in multibody systems. *Multibody System Dynamics*, 16(1):55, Jul 2006.
32. D.P. Townsend. *Dudley's gear handbook*. McGraw-Hill Inc., 2nd edition, 1991.
33. AGMA6123-C16. Design manual for enclosed epicyclic gear drives, 2016.
34. PD McFadden. Window functions for the calculation of the time domain averages of the vibration of the individual planet gears and sun gear in an epicyclic gearbox. *Journal of Vibration and Acoustics*, 116(2):179–187, 1994.
35. A.R. Nejad, Y. Xing, and T. Moan. Gear train internal dynamics in large offshore wind turbines. In *ASME 2012 11th Biennial Conference on Engineering Systems Design and Analysis*, pages 823–831. American Society of Mechanical Engineers, 2012.
36. H. Ormberg and E.E. Bachynski. Global analysis of floating wind turbines: Code development, model sensitivity and benchmark study. In *22nd International Ocean and Polar Engineering Conference*, volume 1, pages 366–373, 2012.
37. IEC 61400-1. Wind turbines, part 1: Design requirements, 2005.
38. L. Li, Z. Gao, and T. Moan. Joint distribution of environmental condition at five european offshore sites for design of combined wind and wave energy devices. *Journal of Offshore Mechanics and Arctic Engineering*, 137(3):031901–(1–16), 2015.
39. E. Hau. *Wind Turbines Fundamentals, Technologies, Application, Economics*. Springer, 2nd edition, 2006.
40. Zhaoqiang Zhang, A. Matveev, S. Øvrebø, R. Nilssen, and A. Nysveen. State of the art in generator technology for offshore wind energy conversion systems. In *2011 IEEE International Electric Machines Drives Conference (IEMDC)*, pages 1131–1136, May 2011.
41. Y. Xing, M. Karimirad, and T. Moan. Modelling and analysis of floating spar-type wind turbine drivetrain. *Wind Energy*, 17:565–587, 2014.
42. W. Dong, Y. Xing, T. Moan, and Z. Gao. Time domain-based gear contact fatigue analysis of a wind turbine drivetrain under dynamic conditions. *International Journal of Fatigue*, 48:133–146, 2013.
43. Z. Jiang, Y. Xing, Y. Guo, T. Moan, and Z. Gao. Long-term contact fatigue analysis of a planetary bearing in a land-based wind turbine drivetrain. *Wind Energy*, 18(4):591–611, 2015.
44. A.R. Nejad, Z. Gao, and T. Moan. On long-term fatigue damage and reliability analysis of gears under wind loads in offshore wind turbine drivetrains. *International Journal of Fatigue*, 61:116–128, 2014.
45. M. Ghane, A.R. Nejad, M. Blanke, Z. Gao, and T. Moan. Condition monitoring of spar-type floating wind turbine drivetrain using statistical fault diagnosis. *Wind Energy*, in press, 2018.
46. P.F. Odgaard and J. Stoustrup. Frequency based fault detection in wind turbines. In *Proceedings of the 19th IFAC World Congress*, pages 5832–5837, Cape Town,South Africa, August 2014.
47. P.F. Odgaard and J. Stoustrup. Gear-box fault detection using time-frequency based methods. *Annual Reviews in Control*, 40:50–58, 2015.

48. Mahdi Ghane, Amir R. Nejad, Mogens Blanke, Zhen Gao, and Torgeir Moan. Diagnostic monitoring of drivetrain in a 5 mw spar-type floating wind turbine using hilbert spectral analysis. *Energy Procedia*, 137:204 – 213, 2017.
49. M. Ghane, A.R. Nejad, M. Blanke, Z. Gao, and T. Moan. Statistical fault diagnosis of wind turbine drivetrain applied to a 5MW floating wind turbine. *Journal of Physics: Conference Series*, 753(5):052017, 2016.
50. Sankar K. Roy, A. R. Mohanty, and C. S. Kumar. Amplitude demodulation of instantaneous angular speed for fault detection in multistage gearbox. In Jyoti K. Sinha, editor, *Vibration Engineering and Technology of Machinery: Proceedings of VETOMAC X 2014, held at the University of Manchester, UK, September 9-11, 2014*, pages 951–961. Springer International Publishing, Cham, 2015.

DOI: 10.1002/we
Prepared using weauth.cls